Electric-permittivity-based instability of two dielectric miscible liquids under DC field

S. Amiroudine[1,a], E. A. Demekhin[2,3,4], V. S. Shelistov[3], and G. S. Ganchenko[3]

[1] Institute of Mechanics and Engineering (I2M) CNRS, University of Bordeaux, 33400 Talence, France
[2] Department of Mathematics and Computer Science, Financial University, Krasnodar, Russian Federation 350051
[3] Laboratory of Micro- and Nanoscale Electro- and Hydrodynamics, Financial University, Krasnodar, Russian Federation 350051
[4] Laboratory of General Aeromechanics, Institute of Mechanics, Moscow State University, Moscow, Russian Federation 119192

Received 7 October 2021 / Accepted 17 December 2021

Abstract This paper considers the mixing of two dielectric miscible viscous liquids with different electric permittivities bounded by solid walls in an external electric field normal to the interface of the liquids. The mutual diffusion of these two liquids leads to the formation of an unsteady self-similar 1D diffusion layer. This layer is found to be unstable to the perturbations of the interface. A special sophisticated mathematical approach in self-similar variables is developed to estimate its stability. The results of a linear stability theory are verified by direct numerical simulations of the full nonlinear problem. A mixing efficiency based on the separation amplitude and an optimal electric field strength to achieve the fastest mixing are proposed in the present study.

1 Introduction

Micro- and nanoscale phenomena of moving conductive and non-conductive liquids with an interface between them are of particular practical interest. Multi-phase flows in micro-scale systems have recently found numerous applications in a wide range of fields like biochemical processing, such as lab-on-chip reactors [1–4], mixers [5,6], DNA extraction [7], drug delivery [8], oil extraction from porous rock formations [9,10]. Miniaturized bioanalytical systems attempt to incorporate many of the necessary components and functionality on the surface of a typical laboratory substrate. Micro Total Analysis Systems (μTAS) components include reaction chambers, pumps, flow sensors, micromixers, diluters, and preconcentrators. Analyses requiring rapid mixing include immunoassays, DNA hybridization, and general cell-molecule interaction. Application of these techniques requires mixing of reagents that have relatively low diffusion coefficients.

Rapid homogeneous mixing becomes increasingly important [11–24]. Such a mixing can be caused by either mechanical vibration through hydrodynamical instability [25–27] or by a special type of hydro-electro instability [28–33]. Electroconvective mixing may result from many physical factors, such as the first kind electroosmotic flow [34], the second kind electroosmotic flow [35,36], buoyant convection [37], conductivity gradient [38], and electric permittivities [39]. The slow diffusion mechanism of mixing is thus complemented by much faster advection mixing.

The electrohydrodynamic instability of liquid flows with conductivity gradients stems from pioneer works by Hoburg and Melcher [28] which are based on classical models by Melcher and Taylor [29] (see also [30,31]). Hoburg and Melcher [28] described the key mechanism of this instability as caused by charge accumulation at the perturbed interface, and made qualitative comparisons of their theory to experiments, but they neglected the diffusion of electric conductivity. As a result, in their calculation, the threshold of instability was absent. This was improved later by Baygents and Baldessari [32] with a more realistic model. However, Baygents and Baldessari [32] wrongly assumed the principle of exchange of stability in their linear stability analysis. This was corrected subsequently by Chang et al. [40] and Sharan et al. [41]. Research on this electrohydrodynamic instability was continued by Santiago's team [16–20,33]. A flow in a long rectangular-cross-section microchannel with a conductity gradient orthogonal to the main flow direction and an external electric field was considered both experimentally and theoretically in [16]. It was found experimentally that such a system exhibits a critical electric field above which the flow is unstable. In the theoretical part, the previous model was generalized in [32]. The volume charge was assumed small enough to be neglected in the ion transport equa-

[a] e-mail: sakir.amiroudine@u-bordeaux.fr (corresponding author)

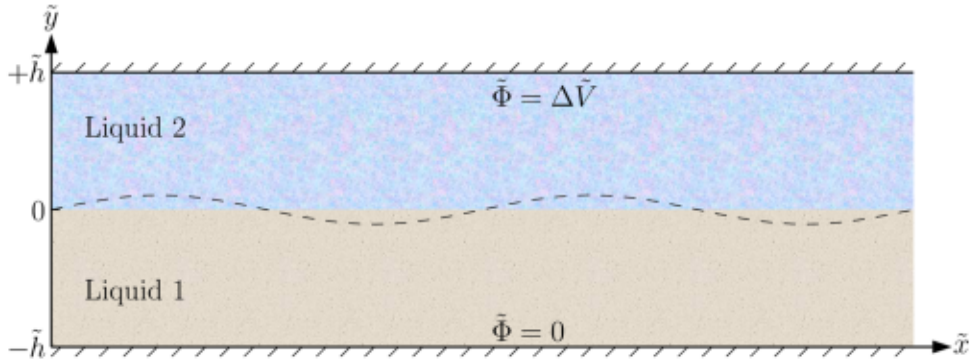

Fig. 1 Schematic of the mixing channel, taken as the computational domain

tions, but not in the equations of fluid motion, where the Coulomb body force, based on the residual charge, was taken into consideration.

A general linear stability analysis of miscible systems is not trivial due to the fact that the base state of the problem is time-dependent and the corresponding linear system ceases to be of classical type. Specifically, the case considered in this paper differs, in two ways, from the usually considered above-mentioned cases of electrohydrodynamic instability: (a) the liquids are dielectrics rather than conductors and, hence, the Maxwell–Wagner stresses are created by the nonuniformity of the dielectric permittivity; (b) the liquids are miscible and the boundary separating them spreads with time by diffusion. These factors make the problem more difficult, but also more interesting. Besides the practical part connected with the desire of reducing the mixing time, this problem raises some fundamental questions, namely, wether it is possible or not to obtain instability in miscible flows with nonuniformly distributed permittivity of these dielectric liquids. To our knowledge, the stability problem of the interface of two viscous miscible liquids with different electric permittivities has not yet been addressed in the past.

The present paper considers a two-phase microflow of dielectric miscible viscous liquids with different electric permittivities bounded by two flat solid walls in an external electric field, normal to the interface. The interface is initially expanding due to diffusion and this process can be described by a self-similar solution. The expanded solution takes into account the nonuniformity of the permittivity of the two liquids which, in principle, can trigger an instability. There is an obvious mathematical difficulty in the solution of the given stability problem: in the self-similar solution, the coefficients of the stability equations depend exponentially on time and an exponential growth rate of the perturbations is thus expected. The classical frozen coefficient approach [42,43] is not applicable in our case. We use sophisticated *ad hoc* method proposed by Shtemler [44] to solve our stability problem. In order to accomplish our investigation and to prove the results of the linear analysis, we apply a numerical integration of the full problem without any simplification. These analytical results are then complemented by direct numerical simulation solutions of the full non-linear problem, and an estimation of the mixing efficiency is proposed as a function of the separation amplitude.

2 Formulation

We consider two viscous miscible dielectric liquids in a $2\tilde{h}$ gap between conducting impermeable walls, see Fig. 1. Notations with tilde are used for the dimensional variables, as opposed to their dimensionless counterparts without tilde. $(\tilde{x}, \tilde{y})$ are the Cartesian coordinates, where $\tilde{x}$ is directed along the channel and $\tilde{y}$ is normal to it.

A potential difference $\Delta\tilde{V}$ is applied between the walls; any external forces (such as gravity), except the electrical one, are neglected. It is assumed that at the initial time, $\tilde{t} = 0$, the interface is a straight line $\tilde{y} = 0$ perturbed with small-amplitude natural "room perturbations" and the first liquid is located in the $-\tilde{h} < \tilde{y} < 0$ region, while the second liquid is in the region $0 < \tilde{y} < \tilde{h}$. These liquids are denoted by the indices of 1 and 2, respectively. At time $\tilde{t} > 0$, the interface is subject to mutual diffusion of these liquids and an electrohydrodynamic instability may arise. The following two-dimensional equations describe the mixture behavior,

$$\tilde{\rho}\left(\frac{\partial w}{\partial \tilde{t}} + \tilde{U}\frac{\partial w}{\partial \tilde{x}} + \tilde{V}\frac{\partial w}{\partial \tilde{y}}\right) = \tilde{D}\left\{\frac{\partial}{\partial \tilde{x}}\left(\tilde{\rho}\frac{\partial w}{\partial \tilde{x}}\right) + \frac{\partial}{\partial \tilde{y}}\left(\tilde{\rho}\frac{\partial w}{\partial \tilde{y}}\right)\right\}, \tag{1}$$

$$\frac{\partial \tilde{\Pi}}{\partial \tilde{x}} - \frac{\partial \tilde{T}_{xx}}{\partial \tilde{x}} - \frac{\partial \tilde{T}_{xy}}{\partial \tilde{y}} = \frac{1}{2}\frac{\partial}{\partial \tilde{x}}\left[\tilde{\varepsilon}\left(\tilde{E}_x^2 - \tilde{E}_y^2\right)\right] + \frac{\partial}{\partial \tilde{y}}\left[\tilde{\varepsilon}\tilde{E}_x\tilde{E}_y\right], \tag{2}$$

$$\frac{\partial \tilde{\Pi}}{\partial \tilde{y}} - \frac{\partial \tilde{T}_{xy}}{\partial \tilde{x}} - \frac{\partial \tilde{T}_{yy}}{\partial \tilde{y}} = \frac{\partial}{\partial \tilde{x}}\left[\tilde{\varepsilon}\tilde{E}_x\tilde{E}_y\right] - \frac{1}{2}\frac{\partial}{\partial \tilde{y}}\left[\tilde{\varepsilon}\left(\tilde{E}_x^2 - \tilde{E}_y^2\right)\right], \tag{3}$$

$$\frac{\partial\left(\tilde{\rho}\tilde{U}\right)}{\partial\tilde{x}}+\frac{\partial\left(\tilde{\rho}\tilde{V}\right)}{\partial\tilde{y}}=0, \tag{4}$$

$$\frac{\partial}{\partial\tilde{x}}\left(\tilde{\varepsilon}\tilde{E}_x\right)+\frac{\partial}{\partial\tilde{y}}\left(\tilde{\varepsilon}\tilde{E}_y\right)=0, \tag{5}$$

where w is the mass fraction of the liquid 1 in the mixture with $0 \le w \le 1$; $\tilde{D}$, $\tilde{\rho}$, $\tilde{\mu}$ and $\tilde{\varepsilon}$ are the diffusion, the density, the dynamic viscosity and the dielectric permittivity of the mixture, respectively; $(\tilde{U}, \tilde{V})$ are the components of the velocity vector, $\tilde{\Pi}$ is the pressure and $\tilde{T}_{ij}$ is the viscous stress tensor. The first equation describes the mixing by diffusion and advection ([45]), the next three equations are Navier–Stokes equations with Maxwell forces in the right-hand side and the continuity equation. The channel is micron-sized and, thus, the Reynolds number is small so that Stokes' approximation for the creeping flow can be applied. The last equation is the Maxwell equation for the electric field which should be completed by the relation, $(\tilde{E}_x, \tilde{E}_y) = -\tilde{\nabla}\tilde{\Phi}$, where $\tilde{\Phi}$ is the electric potential.

In this work, we restrict our analysis to the particular case where the densities of the fluids are equal to each other (this hypothesis will be further verified with experimental data, see Sect. 4.3.4). The liquids are assumed to be Newtonian, but the viscosity $\tilde{\mu}$ of their mixture depends on the mass fraction w, as well as the dielectric permittivity $\tilde{\varepsilon}$. Both dependecies are assumed to be linear functions of w,

$$\begin{aligned}\tilde{\mu} &= \tilde{\mu}_1 w + \tilde{\mu}_2(1-w) = \tilde{\mu}_2 + (\tilde{\mu}_1 - \tilde{\mu}_2)w,\\ \tilde{\varepsilon} &= \tilde{\varepsilon}_1 w + \tilde{\varepsilon}_2(1-w) = \tilde{\varepsilon}_2 + (\tilde{\varepsilon}_1 - \tilde{\varepsilon}_2)w.\end{aligned} \tag{6}$$

The system (1–5) can be rewrittten into the following form,

$$\frac{\partial w}{\partial\tilde{t}}+\tilde{U}\frac{\partial w}{\partial\tilde{x}}+\tilde{V}\frac{\partial w}{\partial\tilde{y}}=\tilde{D}\left(\frac{\partial^2 w}{\partial\tilde{x}^2}+\frac{\partial^2 w}{\partial\tilde{y}^2}\right), \tag{7}$$

$$\frac{\partial}{\partial\tilde{x}}\left(\tilde{\varepsilon}\frac{\partial\tilde{\Phi}}{\partial\tilde{x}}\right)+\frac{\partial}{\partial\tilde{y}}\left(\tilde{\varepsilon}\frac{\partial\tilde{\Phi}}{\partial\tilde{y}}\right)=0, \tag{8}$$

$$\begin{aligned}&\frac{\partial\tilde{\Pi}}{\partial\tilde{x}}+2\frac{\partial}{\partial\tilde{x}}\left(\tilde{\mu}\frac{\partial\tilde{U}}{\partial\tilde{x}}\right)+\frac{\partial}{\partial\tilde{y}}\left(\tilde{\mu}\frac{\partial\tilde{U}}{\partial\tilde{y}}\right)+\frac{\partial}{\partial\tilde{y}}\left(\tilde{\mu}\frac{\partial\tilde{V}}{\partial\tilde{x}}\right)\\ &\quad=-\frac{1}{2}\frac{\partial\tilde{\varepsilon}}{\partial\tilde{x}}\left[\left(\frac{\partial\tilde{\Phi}}{\partial\tilde{x}}\right)^2+\left(\frac{\partial\tilde{\Phi}}{\partial\tilde{y}}\right)^2\right],\end{aligned} \tag{9}$$

$$\begin{aligned}&\frac{\partial\tilde{\Pi}}{\partial\tilde{y}}+2\frac{\partial}{\partial\tilde{y}}\left(\tilde{\mu}\frac{\partial\tilde{V}}{\partial\tilde{y}}\right)+\frac{\partial}{\partial\tilde{x}}\left(\tilde{\mu}\frac{\partial\tilde{U}}{\partial\tilde{y}}\right)+\frac{\partial}{\partial\tilde{x}}\left(\tilde{\mu}\frac{\partial\tilde{V}}{\partial\tilde{x}}\right)\\ &\quad=-\frac{1}{2}\frac{\partial\tilde{\varepsilon}}{\partial\tilde{y}}\left[\left(\frac{\partial\tilde{\Phi}}{\partial\tilde{x}}\right)^2+\left(\frac{\partial\tilde{\Phi}}{\partial\tilde{y}}\right)^2\right],\end{aligned} \tag{10}$$

$$\frac{\partial\tilde{U}}{\partial\tilde{x}}+\frac{\partial\tilde{V}}{\partial\tilde{y}}=0. \tag{11}$$

This system must be complemented by relations (6) and proper boundary conditions (BCs). The solid surfaces $\tilde{y}=\pm\tilde{h}$ are assumed to be impermeable to the mixture, and the no-slip conditions for the velocity are applied at these surfaces. The potential difference $\Delta\tilde{V}$ is applied between the walls. These conditions can be written as follows,

$$\begin{aligned}&\tilde{y}=\pm\tilde{h}: \quad \tilde{U}=\tilde{V}=0, \quad \frac{\partial w}{\partial\tilde{y}}=0;\\ &\tilde{\Phi}\Big|_{\tilde{y}=\tilde{h}}-\tilde{\Phi}\Big|_{\tilde{y}=-\tilde{h}}=\Delta\tilde{V}.\end{aligned} \tag{12}$$

We neglect the net flow along the $\tilde{x}$-direction in order to consider only the impact of electric forces on mixing. The spatial domain is assumed to be infinitely large in the $\tilde{x}$-direction, and the boundedness of the solution as $\tilde{x}\to\pm\infty$ is imposed. Therefore, periodic conditions will be assumed with respect to $\tilde{x}$ in the numerical simulations described in Sect. 4.2.

Adding initial conditions for the fraction w completes the system (7)–(12). At $\tilde{t}=0$,

$$\begin{aligned}&w=1 \quad \text{at} \quad -\tilde{h}<\tilde{y}<0,\\ &w=0 \quad \text{at} \quad 0<\tilde{y}<\tilde{h}\end{aligned} \tag{13}$$

3 Simplified analytical solution

3.1 A one-dimensional self-similar solution

At the initial time $\tilde{t}=0$, liquids 1 and 2 are separated by a sharp boundary at $\tilde{y}=0$. At subsequent moments, $\tilde{t}>0$, mutual diffusion of liquids occurs, which leads to the formation of a thin diffusion layer $\tilde{\delta}(\tilde{t})$. Note that at this period of time, the influence of walls can be neglected and the system has no characteristic size and its solution is thus self-similar.

As long as the diffusion layer is uniform, $\partial/\partial\tilde{x}=0$ and its thickness $\tilde{\delta}$ is a good choice for the dynamic characteristic length, $\tilde{\delta}=2\sqrt{\tilde{D}\tilde{t}}$. The spatial variable $\tilde{y}$ is normalized to $\tilde{\delta}$, and the self-similar variable is introduced as, $\eta=\tilde{y}/\tilde{\delta}$. The derivatives with respect to $\tilde{t}$ and $\tilde{y}$ can be written as,

$$\frac{\partial}{\partial\tilde{t}}=-\frac{\tilde{y}}{4\tilde{t}\sqrt{\tilde{D}\tilde{t}}}\frac{\partial}{\partial\eta}, \quad \frac{\partial}{\partial\tilde{y}}=\frac{1}{2\sqrt{\tilde{D}\tilde{t}}}\frac{\partial}{\partial\eta}. \tag{14}$$

Equation (7) turns into the following ordinary differential equation and BCs,

$$\begin{aligned}&\frac{\mathrm{d}^2 w}{\mathrm{d}\eta^2}+2\eta\frac{\mathrm{d}w}{\mathrm{d}\eta}=0, \quad \eta\to-\infty: \quad w\to 1,\\ &\eta\to+\infty: \quad w\to 0.\end{aligned} \tag{15}$$

The solution of Eq. (15) is a well-known error function,

$$w = \frac{1}{2}\left[1 - \mathrm{erf}(\eta)\right]. \tag{16}$$

The permittivity and the viscosity in the mixing layer can readily be found from relations (6),

$$\begin{aligned}\tilde{\varepsilon} &= \frac{\tilde{\varepsilon}_2 - \tilde{\varepsilon}_1}{2}\mathrm{erf}(\eta) + \frac{\tilde{\varepsilon}_2 + \tilde{\varepsilon}_1}{2},\\ \tilde{\mu} &= \frac{\tilde{\mu}_2 - \tilde{\mu}_1}{2}\mathrm{erf}(\eta) + \frac{\tilde{\mu}_2 + \tilde{\mu}_1}{2}.\end{aligned} \tag{17}$$

By introducing dimensionless parameters β and γ as,

$$\beta = \frac{\tilde{\varepsilon}_1}{\tilde{\varepsilon}_2} - 1, \quad \gamma = \frac{\tilde{\mu}_1}{\tilde{\mu}_2} - 1, \tag{18}$$

we get the dimensionless solution of the permittivity and the viscosity,

$$\varepsilon = \frac{\beta}{2}[1 - \mathrm{erf}(\eta)] + 1, \quad \mu = \frac{\gamma}{2}[1 - \mathrm{erf}(\eta)] + 1. \tag{19}$$

The electric potential $\tilde{\Phi}$ is completely determined from the permittivity field $\tilde{\varepsilon}$ (Eq. 8) and the corresponding BC (Eq. 12),

$$\frac{\partial}{\partial \tilde{y}}\left[\tilde{\varepsilon}\frac{\partial \tilde{\Phi}}{\partial \tilde{y}}\right] = 0, \quad \tilde{\Phi}|_{\tilde{y}=-\tilde{h}} = 0, \quad \tilde{\Phi}|_{\tilde{y}=+\tilde{h}} = \Delta\tilde{V}. \tag{20}$$

This problem is readily solved,

$$\tilde{\Phi} = \tilde{C}\int_{-\tilde{h}}^{\tilde{y}} \frac{\mathrm{d}\tilde{y}}{\tilde{\varepsilon}}, \tag{21}$$

where $\tilde{C}$ is a constant of integration, which is found from the BCs at $\tilde{y} = \pm\tilde{h}$,

$$\Delta\tilde{V} = \tilde{C}\int_{-\tilde{h}}^{+\tilde{h}} \frac{\mathrm{d}\tilde{y}}{\tilde{\varepsilon}} = \tilde{C}\left[\tilde{J} + \tilde{h}\left(\frac{1}{\tilde{\varepsilon}_1} + \frac{1}{\tilde{\varepsilon}_2}\right)\right], \tag{22}$$

in which,

$$\tilde{J} = \int_{-\tilde{h}}^{0}\left(\frac{1}{\tilde{\varepsilon}} - \frac{1}{\tilde{\varepsilon}_1}\right)\mathrm{d}\tilde{y} + \int_{0}^{\tilde{h}}\left(\frac{1}{\tilde{\varepsilon}} - \frac{1}{\tilde{\varepsilon}_2}\right)\mathrm{d}\tilde{y}, \tag{23}$$

We can reduce Eq. (23) to dimensionless form using (14), (18), (19),

$$\Delta\tilde{V} = \tilde{C}\,\frac{2\sqrt{\tilde{D}\tilde{t}}}{\tilde{\varepsilon}_2}\left(J + H\,\frac{2+\beta}{1+\beta}\right), \tag{24}$$

where $H = \tilde{h}/\tilde{\delta}$ and,

$$J = \int_{-H}^{0}\left(\frac{1}{\varepsilon} - \frac{1}{1+\beta}\right)\mathrm{d}\eta + \int_{0}^{H}\left(\frac{1}{\varepsilon} - 1\right)\mathrm{d}\eta. \tag{25}$$

Assuming that $\tilde{\delta} \ll \tilde{h}$, the finite limits of integration can be approximated by infinite ones,

$$J = \int_{-\infty}^{0}\left(\frac{1}{\varepsilon} - \frac{1}{1+\beta}\right)\mathrm{d}\eta + \int_{0}^{\infty}\left(\frac{1}{\varepsilon} - 1\right)\mathrm{d}\eta, \tag{26}$$

which means that J depends only on β, but not on H.

The unknown of integration $\tilde{C}$ can then be deduced from Eq. (24),

$$\tilde{C} = \frac{\tilde{\varepsilon}_2\Delta\tilde{V}}{2\sqrt{\tilde{D}\tilde{t}}}\,\frac{1+\beta}{(2+\beta)H + (1+\beta)J}, \tag{27}$$

with its following dimensionless form,

$$C = \frac{1+\beta}{(2+\beta)H + (1+\beta)J}, \tag{28}$$

where $C = \frac{2\sqrt{\tilde{D}\tilde{t}}}{\tilde{\varepsilon}_2\Delta\tilde{V}}\,\tilde{C}$.

Gravity forces are absent and the problem can thus be taken as symetric and without loss of generality, the bottom and the top liquids can be swapped. Therefore, only positive β can be considered, $J(\beta)$ is evaluated numerically and tabulated (see Table 1).

The hydrodynamics is decoupled from the one-dimensional solution and the velocity components are vanishing (see Eqs. 9–10), but the Coulomb forces produce a nonzero pressure field from Eq. (10). The corresponding solutions for the velocity and pressure field can be written as follows,

$$\tilde{U} = \tilde{V} = 0, \quad \tilde{\Pi} = \frac{1}{4}\tilde{\varepsilon}\left(\frac{\partial\tilde{\Phi}}{\partial\tilde{y}}\right)^2. \tag{29}$$

3.2 Stability of the self-similar solution

The interface between the two liquids is always slightly disturbed by natural "room perturbations". These small disturbances can either decay or grow. In the latter case, the 1D solution is unstable and must evolve into some more complex state, than the one obtained in Sect. 3.1.

We consider the linear stability of the 1D self-similar solution and we slightly perturb it in the $\tilde{x}$-direction. It is more convenient to use different reference values in $\tilde{x}$ and $\tilde{y}$-directions,

$\tilde{l}_0 = 1/\tilde{\alpha}_0$: length in $\tilde{x}$-direction;

Table 1 The function J for different values of β

β	0.10	0.20	0.40	0.70	1.0	2.0	5.0	10.0
J	-0.0035	-0.0121	-0.0383	-0.0870	-0.138	-0.289	-0.580	-0.830

$\tilde{\delta} = 2\sqrt{\tilde{D}\tilde{t}}$: length in $\tilde{y}$-direction;
$\tilde{U}_0 = \tilde{D}/\tilde{l}_0$: velocity in $\tilde{x}$-direction;
$\tilde{V}_0 = \tilde{D}\,\tilde{\delta}/\tilde{l}_0^2$: velocity in $\tilde{y}$-direction;
$\tilde{\Pi}_0 = \tilde{D}\tilde{\mu}_2/\tilde{\delta}^2$: pressure;
$\Delta\tilde{V}$: drop of potential.

Here $\tilde{\alpha}_0$ is some characteristic wavenumber and $\tilde{t}_0$ is some characteristic time (we used $\tilde{t}_0 = \tilde{l}_0^2/\tilde{D}$, but the resulting dimensionless equations do not depend on its choice). New independent variables and their derivatives are introduced,

$$\tau = \frac{\tilde{t}}{\tilde{t}_0}, \qquad \xi = \tilde{x}\tilde{\alpha}_0, \qquad \eta = \frac{\tilde{y}}{\tilde{\delta}} = \frac{\tilde{y}}{2\sqrt{\tilde{D}\tilde{t}}},$$

$$\frac{\partial}{\partial t} = \frac{\partial}{\partial \tau} - \frac{1}{2\tau}\eta\frac{\partial}{\partial \eta}, \qquad \frac{\partial}{\partial \tilde{x}} = \tilde{\alpha}_0\frac{\partial}{\partial \xi}, \tag{30}$$

$$\frac{\partial}{\partial \tilde{y}} = \frac{1}{\tilde{\delta}}\frac{\partial}{\partial \eta}. \tag{31}$$

In self-similar variables, Eq. (7) turns into the following one,

$$4\tau\frac{\partial w}{\partial \tau} - 2\eta\frac{\partial w}{\partial \eta} + \alpha^2\left(U\frac{\partial w}{\partial \xi} + V\frac{\partial w}{\partial \eta}\right) = \alpha^2\left(\frac{\partial^2 w}{\partial \xi^2} + \frac{\partial^2 w}{\partial \eta^2}\right). \tag{32}$$

The dimensionless dielectric permittivity ε and the dimensionless viscosity μ are linear functions of w and can be found from (6),

$$\varepsilon = 1 + \beta w(\tau, \xi, \eta), \qquad \mu = 1 + \gamma w(\tau, \xi, \eta). \tag{33}$$

The electric potential (Eq. 8) turns into,

$$\alpha^2\frac{\partial}{\partial \xi}\left(\varepsilon\frac{\partial \Phi}{\partial \xi}\right) + \frac{\partial}{\partial \eta}\left(\varepsilon\frac{\partial \Phi}{\partial \eta}\right) = 0. \tag{34}$$

The dimensionless parameter $\alpha = \tilde{\delta}\tilde{\alpha}_0$ can have two different interpretations: (i) a dimensionless diffusion length (derived from $\tilde{\delta}$) or (ii) a dimensionless wavenumber (derived from $\tilde{\alpha}_0$). We will use the second choice. This wavenumber depends on time and for sufficiently large time it is assumed to be a slow parameter. The diffusion layer between the two liquids expands exponentially and, therefore, the stability of the self-similar solution cannot be investigated by classical methods as in Refs. [42,43]. The details can be found in Ref. [44], and the corresponding method was successfully applied in [46] and [47]. Details on this will be given later.

Introducing the stream function Ψ from the relations,

$$U = \frac{\partial \Psi}{\partial \eta}, \quad V = -\frac{\partial \Psi}{\partial \xi}, \tag{35}$$

and substituting them into Eqs. (9)–(10), we get,

$$\begin{aligned}&\frac{\partial^2}{\partial \eta^2}\left(\mu\frac{\partial^2 \Psi}{\partial \eta^2}\right) + 4\alpha^2\frac{\partial^2}{\partial \xi \partial \eta}\left(\mu\frac{\partial^2 \Psi}{\partial \xi \partial \eta}\right) + \alpha^4\frac{\partial^2}{\partial \xi^2}\left(\mu\frac{\partial^2 \Psi}{\partial \xi^2}\right)\\ &\quad -\alpha^2\frac{\partial^2}{\partial \xi^2}\left(\mu\frac{\partial^2 \Psi}{\partial \eta^2}\right) - \alpha^2\frac{\partial^2}{\partial \eta^2}\left(\mu\frac{\partial^2 \Psi}{\partial \xi^2}\right)\\ &= \Lambda\frac{\partial \varepsilon}{\partial \xi}\left(\frac{\partial \Phi}{\partial \eta}\frac{\partial^2 \Phi}{\partial \eta^2} + \alpha^2\frac{\partial \Phi}{\partial \xi}\frac{\partial^2 \Phi}{\partial \xi \partial \eta}\right)\\ &\quad -\Lambda\frac{\partial \varepsilon}{\partial \eta}\left(\frac{\partial \Phi}{\partial \eta}\frac{\partial^2 \Phi}{\partial \xi \partial \eta} + \alpha^2\frac{\partial \Phi}{\partial \xi}\frac{\partial^2 \Phi}{\partial \xi^2}\right).\end{aligned} \tag{36}$$

Here, the parameter, $\Lambda = \frac{\tilde{\varepsilon}_2\Delta\tilde{V}^2}{\tilde{D}\tilde{\mu}_2}$ is introduced. It characterises the coupling between hydrodynamics and electrostatics and for fixed physical properties, it corresponds to the square of the dimensionless potential drop.

Imposing small perturbations on the 1D self-similar solution, substituting them into Eqs. (32)–(36) and linearizing with respect to the perturbations turns this system into a linear system with the coefficients independent of the coordinate ξ. It allows seeking sinusoidal elementary solution with respect to ξ-coordinate but its dependence on time must be changed from exponential to the power one. The reason comes from the fact that in this linear stability analysis, the coefficient of the time derivative depends itself on time [$4\tau\frac{\partial w}{\partial \tau}$ in Eq. (32)]. As a result, the linear perturbations will not grow exponentially with time, as we used to have in most of the classical linear stability hydrodynamic problems, but in form of power law in time,

$$w = w_0(\eta) + \hat{w}(\eta)e^{i\xi}\tau^{\lambda}, \quad \Phi = \Phi_0(\eta) + \hat{\Phi}(\eta)e^{i\xi}\tau^{\lambda},$$
$$\Psi = -i\hat{\Psi}(\eta)e^{i\xi}\tau^{\lambda}, \tag{37}$$

where subscript 0 refers to the 1D self-similar solution and λ is the growth rate. The factor $-i$ before the amplitude of the stream function is introduced in order to make all the system coefficients real. Upon substitution of the expressions (37) into Eqs. (32), (34) and (36), omitting the subscript '0' and after linearization, we get the following system of ODEs,

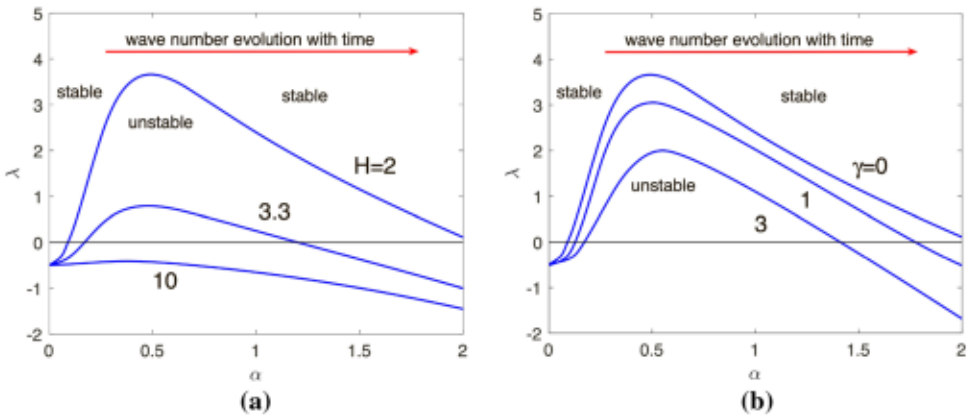

Fig. 2 Growth rate λ vs the wavenumber α for **a** $\Lambda = 1500$, $\beta = 2.25$ and $\gamma = 0$ and different values of the dimensionless half-width of the channel H and, **b** $\Lambda = 1500$, $H = 2$ and different values of dimensionless viscosity γ

$$4\lambda\hat{w} - 2\eta\hat{w}' + \alpha^2 w'\hat{\Psi} = \hat{w}'' - \alpha^2\hat{w}, \tag{38}$$

$$(\varepsilon\hat{\Phi}' + \hat{\varepsilon}\Phi')' - \alpha^2\varepsilon\hat{\Phi} = 0, \tag{39}$$

$$\mu\left(\hat{\Psi}^{IV} - 2\alpha^2\hat{\Psi}'' + \alpha^4\hat{\Psi}\right) + \gamma\left(w''\hat{\Psi}'' + 2w'\hat{\Psi}''' - 2\alpha^2 w'\hat{\Psi}' + \alpha^2 w''\hat{\Psi}\right) = \Lambda\Phi'(\hat{\varepsilon}\Phi'' - \hat{\Phi}'\varepsilon'), \tag{40}$$

where the prime means the derivative with respect to η. The BCs are,

$$\hat{w} = 0, \quad \hat{\Phi} = 0, \quad \hat{\Psi} = 0, \quad \hat{\Psi}' = 0 \text{ at } \eta = H. \tag{41}$$

Here from the self-similar solution,

$$\varepsilon = 1 + \frac{\beta}{2}[1 - \mathrm{erf}(\eta)] + 1, \quad \mu = 1 + \frac{\gamma}{2}[1 - \mathrm{erf}(\eta)] + 1,$$
$$\Phi' = C(H,\beta)\frac{1}{\varepsilon}. \tag{42}$$

The formulated spectral stability problem is described by four outer parameters, β, γ, H and Λ and one inner parameter, the wavenumber, α ($C(H,\beta)$ is defined via $J(\beta)$ (see Eq. 28) and is presented in Table 1). Note that β characterizes the ratio of the permittivity of the two liquids, γ is the ratio of their viscosity, Λ is the normalized strength of the electric field, H and α are slowly changing parameters with time.

The eigenvalue problem for the growth rate λ was solved numerically by the shooting method, using λ as a parameter, conditions (41) at $\eta = -H$ as the initial conditions for the Cauchy problem and the corresponding conditions at $\eta = +H$ as the target.

The dependence of the growth rate λ on the wavenumber α for equal viscosity of liquids $\gamma = 0$ for different dimensionless channel widths $H = \tilde{h}/\tilde{\delta}$ is presented in Fig. 2a. The influence of different viscosities on the dependence $\lambda(\alpha)$ is shown in Fig. 2b. Increasing the value of $\gamma = \tilde{\mu}_1/\tilde{\mu}_2 - 1$ leads to a system which is more and more stable. Note that for equal liquid permittivity $\beta = 0$ the flow is stable for any value of other parameters. This fact allows us calling this instability as the electric-permittivity-based instability which corresponds to a new type of instability in miscible fluids.

According to the classification of Cross and Hohenberg [48], the instability described above is a short-wave instability: the long waves and the very short waves are stable, while the intermediate ones are unstable. This classification determines the behavior of the perturbations in time. The peculiarity of our case is that while the dimensional wavenumber $\tilde{\alpha}$ and the channel width $\tilde{h}$ are fixed, their dimensionless counterparts $\alpha = \tilde{\alpha}\tilde{\delta}$ and $H = \tilde{h}/\tilde{\delta}$ are slowly changing in time. The fact that H and α are time-dependent is justified both experimentally and in numerical simulations. In Fig. 3 the results are presented in the coordinates,

$$\frac{1}{H} = \frac{2}{\tilde{h}}\sqrt{\tilde{D}\tilde{t}}, \quad \alpha = 2\tilde{\alpha}_0\sqrt{\tilde{D}\tilde{t}},$$

for different fixed parameters Λ and β, which are independent of time.

The ratio $k = \alpha/H^{-1}$ does not depend on time, but the position of the point on this k-line depends on time. Each straight line, emanating from the origin $(0,0)$, with the inclination k, $\left(\alpha = k\,\frac{1}{H}\right)$, characterizes the scenario of the time evolution of the imposed perturbation with dimensional and constant in time wavenumber $\tilde{\alpha}_0$. The point $(1/H, \alpha)$ on each straight line moves away from the origin as a square root of time, $\sqrt{\tilde{t}}$.

For sufficiently large $k > k^*$ (which corresponds to short waves) the straight line with inclination k will be in the stable region. The corresponding perturbation on the entire line will decay. For $k < k^*$ (intermediate and long waves), the straight line will cross the unstable region, but at small times, the perturbation will always decay, reflecting the short-wave instability. For the marginal case, $k = k^*$, the straight line only touches the instability region, but does not cross it. Hence, this results in a rather sophisticated behavior. Depending on the value of k, two different scenarios are possible: (a) stable, when the perturbation always decays; (b) unstable, when the perturbation originally decays, then grows and eventually decays again. Such behavior will be confirmed later in our direct numerical simulation.

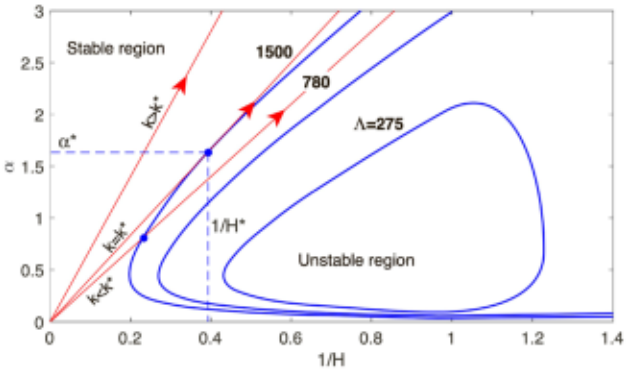

Fig. 3 Marginal stability curves for $\beta = 2.25$ and $\gamma = 0$ in coordinates α–$1/H$. The wavenumber α and $1/H$ are changing along the straight line as it is shown by the red arrows; λ during this evolution successively transfers between stable, unstable and again stable regions

4 Direct numerical simulation

To make the analysis complete, the 1D self-similar analytic solution and its stability investigation are supplemented by the direct numerical simulation (DNS) of the full nonlinear problem.

4.1 Dimensionless equations

In order to render the system dimensionless, the following characteristic quantities are chosen in our direct numerical simulations,

$\tilde{h}$: half-width of the channel;
$\tilde{h}^2/\tilde{D}$: time;
$\tilde{U}_0 = \tilde{D}/\tilde{h}$: velocity;
$\tilde{\Pi}_0 = \tilde{D}\tilde{\mu}_2/\tilde{h}^2$: pressure;
$\tilde{\varepsilon}_2$: permittivity of the fluid 2;
$\Delta\tilde{V}$: drop of potential over the channel width.

Unlike Sect. 3, we select a time-independent characteristic width here, which will simplify the interpretation of the results. The problem is described by the following dimensionless equations,

$$\frac{\partial w}{\partial t} + U\frac{\partial w}{\partial x} + V\frac{\partial w}{\partial y} = \frac{\partial^2 w}{\partial x^2} + \frac{\partial^2 w}{\partial y^2}, \tag{43}$$

$$\frac{\partial}{\partial x}\left(\varepsilon\frac{\partial \Phi}{\partial x}\right) + \frac{\partial}{\partial y}\left(\varepsilon\frac{\partial \Phi}{\partial y}\right) = 0, \tag{44}$$

$$-\frac{\partial \Pi}{\partial x} + 2\frac{\partial}{\partial x}\left(\mu\frac{\partial U}{\partial x}\right) + \frac{\partial}{\partial y}\left(\mu\frac{\partial U}{\partial y}\right) + \frac{\partial}{\partial y}\left(\mu\frac{\partial V}{\partial x}\right) = \frac{\Lambda}{2}\frac{\partial \varepsilon}{\partial x}\left[\left(\frac{\partial \Phi}{\partial x}\right)^2 + \left(\frac{\partial \Phi}{\partial y}\right)^2\right], \tag{45}$$

$$-\frac{\partial \Pi}{\partial y} + 2\frac{\partial}{\partial y}\left(\mu\frac{\partial V}{\partial y}\right) + \frac{\partial}{\partial x}\left(\mu\frac{\partial U}{\partial y}\right) + \frac{\partial}{\partial x}\left(\mu\frac{\partial V}{\partial x}\right) = \frac{\Lambda}{2}\frac{\partial \varepsilon}{\partial y}\left[\left(\frac{\partial \Phi}{\partial x}\right)^2 + \left(\frac{\partial \Phi}{\partial y}\right)^2\right], \tag{46}$$

$$\frac{\partial U}{\partial x} + \frac{\partial V}{\partial y} = 0. \tag{47}$$

The BCs are,

$$y = \pm 1: \quad U = V = 0, \quad \frac{\partial w}{\partial y} = 0;$$
$$\Phi|_{y=+1} - \Phi|_{y=-1} = 1. \tag{48}$$

and initial conditions are as follows,

$$t = 0: \quad w = 1 \quad \text{at} \quad -1 < y < 0,$$
$$w = 0 \quad \text{at} \quad 0 < y < 1, \tag{49}$$

where small perturbations in the x-direction on the interface are assumed to be superimposed on this BC.

The problem is characterized by three dimensionless parameters: β, γ and Λ, all defined previously in Sect. 3. The latter can be rewritten as,

$$\Lambda \equiv \frac{\tilde{\varepsilon}_2 \Delta\tilde{V}^2}{\tilde{D}\tilde{\mu}_2} = \frac{\Delta\tilde{V}^2}{\tilde{D}\tilde{\mu}_2/\tilde{\varepsilon}_2} = \frac{\Delta\tilde{V}^2}{\Delta\tilde{V}_0^2},$$

which represents the square of the dimensionless drop of the electric potential with the electroviscous potential $\Delta\tilde{V}_0 = \sqrt{\tilde{D}\tilde{\mu}_2/\tilde{\varepsilon}_2}$.

In order to distinguish between dimensionless wavenumbers defined in the self-similar analysis and the present DNS model, we denote the wavenumber here as $k = \tilde{\alpha}\tilde{h}$ in contrast to $\alpha = \tilde{\alpha}\tilde{\delta}$ in the self-similar basis, so that $k = \frac{\alpha}{1/H}$, where $H = \tilde{h}/\tilde{\delta}$.

Note that k is a dimensionless wave number in the present basis not only but has also another meaning: it represents the inclination as defined in Sect. 3 (see Fig. 3).

Besides, if we consider the dependence between α, k and t, then $\alpha^2 = \tilde{\alpha}^2 4\tilde{D}\tilde{t}$ or $\alpha^2 = 4k^2 t$ and we can then obtain the following useful relation,

$$t = \frac{\alpha^2}{4k^2}. \tag{50}$$

The problem is solved for the following physical properties (the same viscosity has been taken for both fluids for the sake of comparison with the analytical solution): $\tilde{\mu}_1 = \tilde{\mu}_2 = 1 \times 10^{-3}$ kg/(m s), $\tilde{D} \approx 10^{-9}$ m^2/s, $\tilde{\varepsilon}_2 = 2 \times 10^{-10}$ C^{2}s^2/(kg m^3), $\Delta\tilde{V}_0 = 0.097$ V. $\beta = 2.25$ is used in computations. These properties loosely correspond to water ($\tilde{\varepsilon}_1$) and ethanol ($\tilde{\varepsilon}_2$).

The potential drop is varied within $\Delta\tilde{V} = 0$–20 V. Thus, the dimensionless parameter Λ changes from 0 to 42,500.

The case of different viscosity will be used in Sect. 4.3.4 for sake of comparison with experimental data.

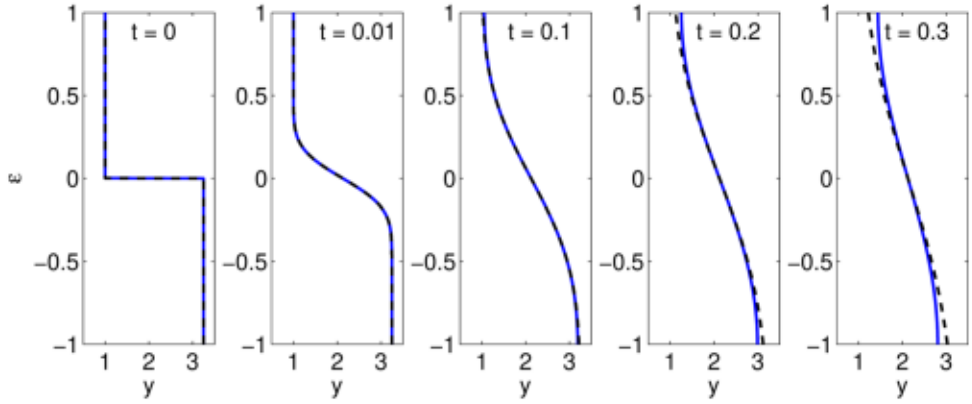

Fig. 4 Evolution of the 1D permittivity solution for different time instants with $\beta = 2.25$. Solid line stands for the DNS and dashed line, for the analytical solution (Eq. 27)

4.2 Numerical methodology

The numerical solution is based on the finite-difference method proposed in [49]. The space derivatives are approximated by a two-point difference scheme of the second order on a staggered grid. Spatial discretization with fine resolution leads to stiff problems and requires implicit methods for time advancement. Fully implicit methods produce a set of nonlinear coupled equations for the problem variables on the new time level, and are usually prohibitively costly for long-term calculations of the multi-parameter problems. Semi-implicit methods, in which only a part of the operator is treated implicitly, constitute a reasonable compromise for this class of problems. The semi-implicit third-order Runge-Kutta method [50] is used for time integration. The functions Φ and Ψ are found by a direct solution of the sparse system of linear algebraic equations, directly following from the discretization of the equations.

The infinite spatial domain is modelled by a finite domain that has dimensionless length l (so that waves with wavenumbers starting from $k_{\min} = 2\pi \ / \ l$ can be captured in simulations). The condition that the solution at $x \to \infty$ is bounded, is changed to periodic boundary conditions. The length of the domain has to be taken large enough to make the solution independent of the domain size. The value $l = 4\pi$ was typically chosen in most calculations, whereas $l = 8\pi$ was used to verify the results.

4.3 Results

4.3.1 Linear stage of evolution

For subcritical values of Λ and β, all perturbations in x-direction decay and the 1D solution is observed. However, this solution does not fully correspond to the self-similar solution due to the influence of the walls that breaks down the validity of the latter. The dimensionless time of the order of $\tilde{t} \sim 0.1 \ \frac{\tilde{h}^2}{D}$ still provides perfect matching between self-similar and DNS solutions when representing the permittivity as a function of the y-direction, see Fig. 4. The dimensionless time of full mixing is estimated of the order $t \sim 0.5$. Evidently, the diffusion is the only one mechanism to mix the two fluids for the 1D solution.

Small perturbations are superimposed on the interface between the liquids in the numerical simulations. Two kinds of such perturbations are considered:

(a) The initial disturbances which are natural from the viewpoint of the experiment. The so-called "room perturbations" determining the external low-amplitude and broadband white noise are imposed on the surface.

(b) Artificial forced monochromatic perturbations with a fixed wavenumber $\tilde{\alpha}$. These artificial perturbations allow better understanding of the behavior of the system.

For the supercritical parameters, a special kind of electro-hydrodynamical instability takes place. The instability triggers an additional mechanism of mixing, by advection, which is more powerful and strongly reduces the time for mixing. In all subsequent calculations, the initial conditions are defined as follows for both monochromatic and room perturbations,

$$w_0 = \frac{1}{2}\left(1 - \operatorname{sign}(y)\right) + A_0\left(1 - \left|\tanh(ay)\right|\right)\left(\operatorname{sign}(y) + s(x)\right),$$

where $s(x)$ is either a uniformly distributed random value in the range $[-1,+1]$, or a monochromatic sinusoidal wave. We define the following function (which will be also used in Sect. 4.3.2),

$$A(t) = \max_{(y)}\left(\max_{(x)} w(t,x,y) - \min_{(x)} w(t,x,y)\right).$$

$A_0 = A(0)$ is a small parameter specifying the amplitude of disturbances, and 'a' controls the initial mixing layer thickness. Numerical simulations were performed with $a = 99$.

Let us first consider simulations for the monochromatic perturbations as initial conditions. For such conditions, the initial perturbation is set up by a sinusoidal perturbation in x-direction with one single wavenumber k. These perturbations are artificial, but they allow us to understand the nature of the instability. So we return to the interpretation of the results of our self-similar analysis in Fig. 3. Keeping the wave number

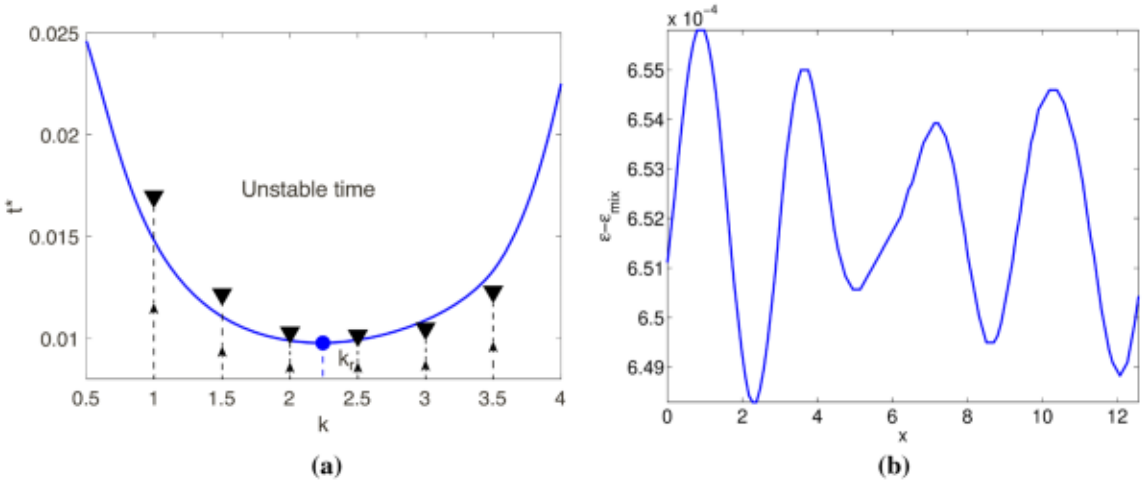

Fig. 5 **a** Solid line stands for the marginal stability of the self-similar solution, triangles (DNS simulations) stand for the time when monochromatic perturbations with the wavenumber k change their decay to growth. The filled circles stand for the wavenumber k_r realized for the room disturbances as intitial conditions, $\beta = 2.25$ and $\Lambda = 1500$; **b** Permittivity at the cross-section ($y = 0$) for $\Lambda = 1500$, $\beta = 2.25$, $\varepsilon_{\text{mix}} = 1 + \beta/2$ is the permittivity of the mixture. The disturbances are fully developed, $t \approx 0.14$

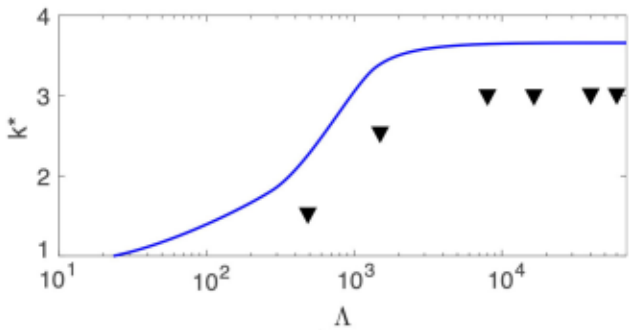

Fig. 6 Marginal stability wavenumber k^* vs Λ for $\beta = 2.25$. Solid line corresponds to the self-similar solution and triangles for the DNS solution

k constant, originally along the straight line in Fig. 3, the disturbance decays first and after some time it may grow. As it can be seen from Fig. 5a even for the unstable parameters there is a latent period of time when perturbations do not grow up to a certain time. These observations are in good correspondence with the linear analysis of the self-similar solutions (see Fig. 5a).

The second kind of perturbations is the natural "room disturbances". In our case, all other perturbations practically decay in comparison with the most dangerous one with the wavenumber k_r, see Fig. 5a. Thus, any evolution results in an almost monochromatic perturbation with the wavenumber k_r. It is close to the wavenumber observed in DNS (Fig. 5b).

The results of the numerical simulation of the nonlinear system (43)–(49) with the natural white noise initial conditions are in good correspondence with the linear stability results. Both are presented in Fig. 6.

4.3.2 Nonlinear evolution

The linear filtering mechanism singles out only one wave number k_r with minimal time to instability, see Fig. 5a. When the amplitude of the perturbation becomes sufficiently large, the nonlinear stage of evolution takes place.

For monochromatic disturbances, the function $A(t)$ (defined in Sect. 4.3.1) is two times the amplitude of those disturbances. It is easy to see that $A(t)$ is exactly zero for any 1D solution (including fully mixed state), and the range of its possible values is $[0, 1]$. The maximal value, 1, is reached when both pure liquids 1 and 2 are present at some $y = \text{const}$. The temporal evolution of the amplitude as a function of its initial value and of the voltage is shown in Fig. 7. After the initial stage, which, in accordance to the linear stability analysis, consists of a characteristic decay and followed by a growth, the disturbances reach saturation and then decay again. This decay seemingly justifies the picture in Fig. 2b, where all perturbations decay at sufficiently large times. In reality, the mechanisms differ. On the one hand, for a long-time process the perturbations are always nonlinear: the interface between the two phases becomes too bent for linearization to be valid. On the other hand, the diffusion smooths out the difference in concentration of the two liquids. The final stage of the evolution corresponds to the uniformly distributed (fully mixed) fluids.

If the potential difference is large enough, $\Lambda > \Lambda^*$ (approximately 5000), the amplitude can reach unity, i.e. the system contains areas filled with pure liquids 1 and 2 along some y-cross-section. Calculations show that these areas extend in "stripes" to almost the full microchannel width (Fig. 8e), and in this case the diffusion process occurs along x (Fig. 8f). For $\Lambda < \Lambda^*$, transverse diffusion develops for sufficiently long time

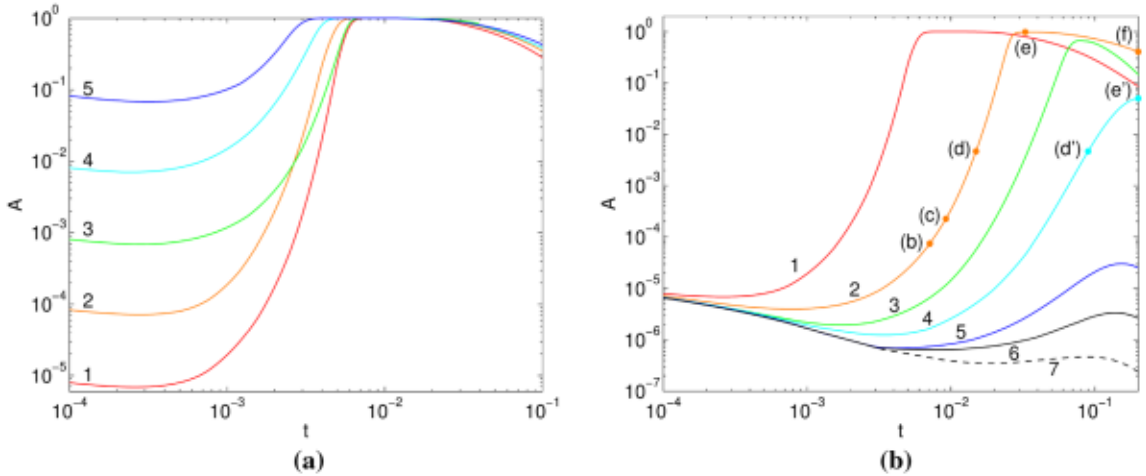

Fig. 7 Development of $A(t)$ as a function of **a** initial amplitude A_0 (1—$A_0 = 10^{-5}$, 2—10^{-4}, 3—10^{-3}, 4—10^{-2}, 5— 10^{-1}) and for $\beta = 2.25$ and $\Lambda = 37000$, **b**Λ: 1—$\Lambda = 37{,}000$, 2—16,500, 3—6100, 4—4000, 5—2500, 6—1500, 7—1000, $A_0 = 10^{-5}$. The marked points are depicted in Fig. 8

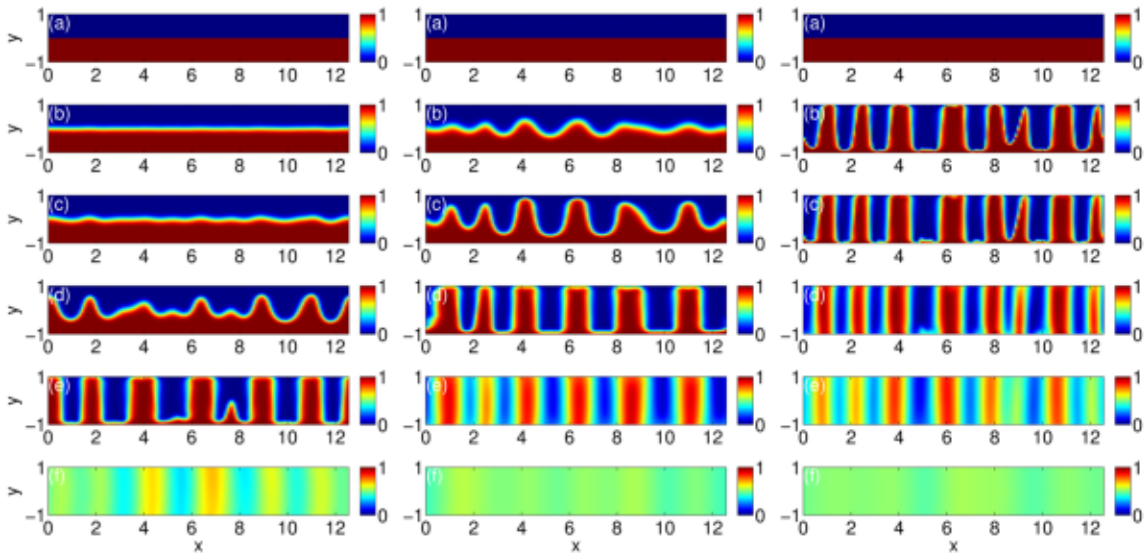

Fig. 8 Temporal development of the fraction w for fluid 1 for $\beta = 2.25$, $A_0 = 10^{-5}$. **a** $t = 0$, **b** 0.0071, **c** 0.0092, **d** 0.0149, **e** 0.0328, **f** 0.2. Snapshots (**b**–**f**) correspond to the markers in Fig. 7. Left column: $\Lambda = 16{,}500$, center column: $\Lambda = 32{,}000$, right column: $\Lambda = 65{,}500$

(see Fig. 9d′) and the concentration gradient does not reach sufficient high values to form "stripes" (Fig. 9e′).

4.3.3 Mixing efficiency

In order to estimate mixing efficiency, we introduce the separation amplitude,

$$A_{\mathrm{sep}}(t) = \frac{1}{x_{\max}} \iint \left| w - \frac{1}{2} \right| \mathrm{d}x\mathrm{d}y, \qquad (51)$$

where the integration is performed over the whole simulation domain. This amplitude also varies from 0 to 1, where '0' means complete mixing and '1' means complete separation.

Our calculations (Fig. 10) show that the mixing efficiency practically does not depend on Λ unless it is large enough, $\Lambda > \Lambda^*$. As mentioned earlier, the value of Λ^* is connected with the appearance of the "stripes", so these "stripes" are responsible for mixing enhancement over low-voltage regimes. However, with increasing Λ, this enhancement becomes small.

The dynamics of the solution in time sequentially goes through four stages:

I. A self-similar expansion of the diffusion layer according to Eq. (16) occurs. The solution does not depend on the strength of the external electric field and is determined only by the diffusion of the two layers. If we take the characteristic time associated with diffusion $\tilde{t}_D = \tilde{h}^2/\tilde{D}$, then the curves in Fig. 10 shrink into one line and Eq. (51) for

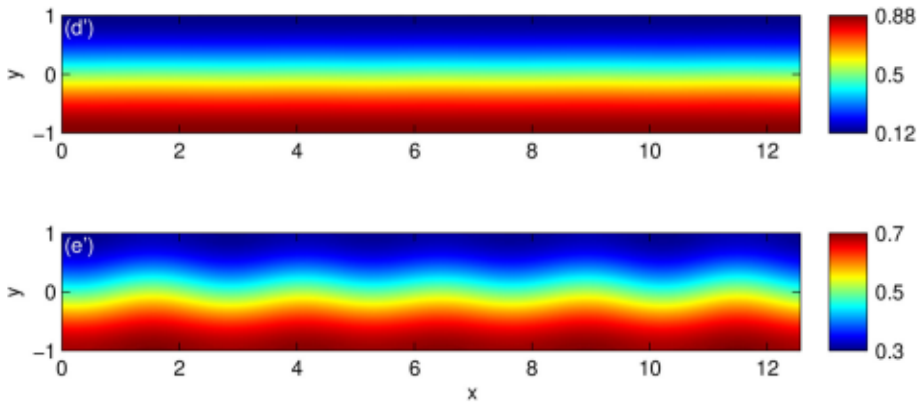

Fig. 9 Temporal development of the fraction w for fluid 1: $\beta = 2.25$, $\Lambda = 4000$, $A_0 = 10^{-5}$. The snapshots are marked in Fig. 7

self-similar solution (16) can be written as,

$$A_{\rm sep}(t) = \mathrm{erf}\left(\frac{1}{2\sqrt{t}}\right) + 2\sqrt{\frac{t}{\pi}}\left(\exp\left(-\frac{1}{4t}\right) - 1\right). \tag{52}$$

II. If the external field is strong enough, then the self-similar solution loses its stability. The initial disturbances grow until the velocity components become large enough.

III. At some time $t = t^*$, the disturbances become large enough to affect the convective terms and, hence, $A_{\rm sep}$. For $t > t^*$ it is convenient to switch to a different characteristic time, namely, $\tilde{t}_c = \frac{\tilde{\mu}_2^2 \tilde{h}_0^2}{\tilde{\varepsilon}_2 \Delta \tilde{V}^2}$. With this time, the parameter Λ disappears from the right hand-side of Eqs. (45–46) but appears on the right-hand side of the diffusion-convection equation of the fraction w (Eq. 43),

$$\frac{\partial w}{\partial t} + U\frac{\partial w}{\partial x} + V\frac{\partial w}{\partial y} = \frac{1}{\Lambda}\left(\frac{\partial^2 w}{\partial x^2} + \frac{\partial^2 w}{\partial y^2}\right). \tag{53}$$

For $\Lambda \to \infty$, the solution of the system of equations does not depend on Λ and all curves (see Fig. 10) shrink into one. The diffusion is negligible for this case.

IV. Diffusion of the formed regular structures. As the liquids are mixing at stage III, the "stripes" of the fraction w are eventually formed, where w practically does not depend on the y-coordinate, see Fig. 8. Also, $\mathrm{d}w/\mathrm{d}y = 0$ at the horizontal boudaries, so the velocity field vanishes, $U = V = 0$. Mixing is thus carried out only by the diffusion, hence the diffusion time $\tilde{t}_D = \tilde{h}^2/\tilde{D}$ must be taken as the characteristic one. Curves 1, 2 and 3 turn into parallel straight lines in semilogarithmic coordinates, see inset of Fig. 10a.
It is possible to show it with trivial case. If we consider the diffusion problem and keep only the main harmonics in the series along x with wavenumber k,

$$w_0 = \frac{1}{2}(\cos(kx) + 1), \tag{54}$$

then this problem can be solve analytically and $A_{\rm sep}$ takes the following form,

$$A_{\rm sep} = \frac{2}{\pi}\exp\left(-k^2 t\right). \tag{55}$$

One can see that the dotted line in Fig. 10 is parallel to the others with non-zero Λ. It means that curves differ only by a multiplication constant, which transform into an additive constant in the logarithmic scale.

4.3.4 Mechanism of the instability

In order to understand the physical mechanism of the instability shown in Fig. 7, we consider a simplified theory. Note that there two competitive time-dependent phenomena in this process are: (i) the mixing length when the diffusion layer is expanding in the $\tilde{y}$-direction as $2\sqrt{\tilde{D}\tilde{t}}$ and (ii) the amplitude of the unstable perturbation in the x-direction which is increasing in time. The first one depends only on the diffusivity ($\tilde{D}$) and does not depend on the voltage ($\Delta\tilde{V}$) and the second depends strongly on $\Delta\tilde{V}$ and with its increase, the growth rate also increases. For sufficiently large $\Delta\tilde{V}$, the first characteristic time is much slower than the second one and, qualitatively, the instability can be considered with some frozen constant $\tilde{\delta}$. This is well illustrated in Fig. 7 in which one can see that the mixing layer is practically not changing with time while the instability runs into the non-linear phase of its evolution. The second assumption of this simplified theory is that we restrict ourselves with the long-wave perturbations.

The instability is connected with the ratio of permittivity $\tilde{\varepsilon}_1/\tilde{\varepsilon}_2$ which is taken as very large. Hence, our assumptions are the following,

$$(a)\quad \Delta\tilde{V} \gg \Delta\tilde{V}_0, \quad \Delta\tilde{V}_0 = \sqrt{\tilde{D}\tilde{\mu}_2/\tilde{\varepsilon}_2},$$
$$(b)\quad \partial/\partial\tilde{x} \ll \partial/\partial\tilde{y},$$
$$(c)\quad \tilde{\varepsilon}_1/\tilde{\varepsilon}_2 \gg 1.$$

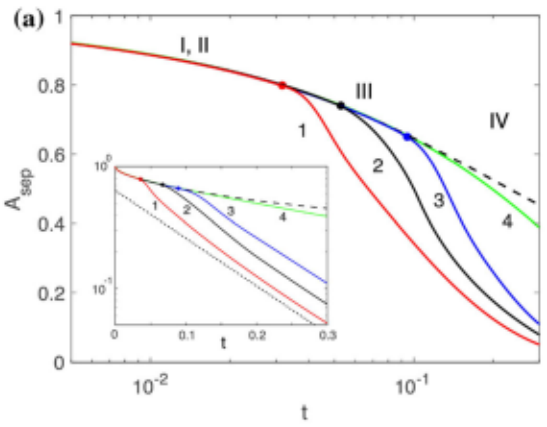

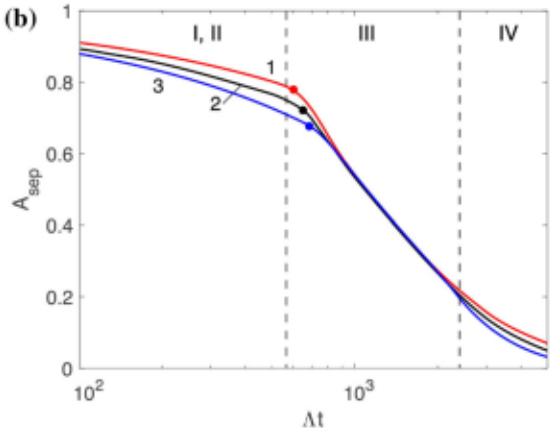

Fig. 10 Separation amplitude dynamics for different Λ and $\beta = 2.25$as a function **a** of time, and **b** Λt. 1: $\Lambda = 16{,}500$, 2: 13,000, 3: 8100, 4: 0. Dashed line corresponds to the self-similar solution (Eq. 51). Dotted line corresponds to the diffusion of vertical structures (53) in region IV with $k = 3$

Let us consider the permittivity dependence as a piecewise linear function,

$$\tilde{\varepsilon} = \begin{cases} \tilde{\varepsilon}_1 & \text{for} \quad -\tilde{h} < \tilde{y} < \tilde{\Delta}_1, \\ \frac{\tilde{\varepsilon}_1+\tilde{\varepsilon}_2}{2} + \frac{\tilde{\varepsilon}_1-\tilde{\varepsilon}_2}{\tilde{a}}(\tilde{y}-\tilde{a}) & \text{for} \quad \tilde{\Delta}_1 < \tilde{y} < \tilde{\Delta}_2, \\ \tilde{\varepsilon}_2 & \text{for} \quad \tilde{\Delta}_2 < \tilde{y} < \tilde{h}. \end{cases} \quad (56)$$

where $\tilde{\Delta}_1 = -\tilde{\delta}/2 + \tilde{a}(\tilde{x},\tilde{t})$ and $\tilde{\Delta}_2 = \tilde{\delta}/2 + \tilde{a}(\tilde{x},\tilde{t})$ (see Fig. 11 for details). Under the above assumptions, Eq. (8) can be integrated twice and the constants of integration can readily been found from the BCs, Eq. (12),

$$\partial\tilde{\Phi}/\partial\tilde{y} \equiv \tilde{E} = \frac{\tilde{\varepsilon}_2\Delta\tilde{V}}{\tilde{h}}\frac{B}{\tilde{\varepsilon}}, \quad (57)$$

where B is a dimensionless constant of integration which is given by,

$$B = \left[1 - \frac{1}{2}\frac{\tilde{\delta}}{\tilde{h}} + \frac{\tilde{\delta}}{\tilde{h}}\frac{\ln\tilde{\varepsilon}_1/\tilde{\varepsilon}_2}{\tilde{\varepsilon}_1/\tilde{\varepsilon}_2} - \frac{\tilde{\varepsilon}_1}{\tilde{\varepsilon}_2}\frac{\tilde{a}(\tilde{x},\tilde{t})}{\tilde{h}}\right]^{-1}. \quad (58)$$

The terms connected with velocity $\tilde{V}$ and $(\partial\tilde{\Phi}/\partial\tilde{x})^2$ can be omitted and the Maxwell pressure $\tilde{\Pi}$ can be found from Eq. (10). Moreover, by simple algebra, we can show that, $\tilde{\Pi}_2/\tilde{\Pi}_1 = \tilde{\varepsilon}_1/\tilde{\varepsilon}_2 \gg 1$. In accordance with the hypothesis (c), $\tilde{\Pi}_1$ can be neglected in comparison with $\tilde{\Pi}_2$. Hence, the pressure field $\tilde{\Pi}_2$ can be calculated from Eq. (10) and Eq. (51) with the above assumptions,

$$\tilde{\Pi}_2 = \frac{1}{2}\frac{\tilde{\varepsilon}_2^2\Delta\tilde{V}^2}{\tilde{h}^2}B^2. \quad (59)$$

The Maxwell pressure $\tilde{\Pi}_2$ is directly proportional to the squared voltage and inversely proportional to the width of the channel $\tilde{h}$ (the smaller is the width of the channel, the larger is $\tilde{\Pi}_2$). Note also that $\tilde{\Pi}_2(\tilde{x},\tilde{t})$ has a maximum which coincides the maximum of $\tilde{a}(\tilde{x},\tilde{t})$, the same applies with the minimum. Thus if the layer of liquid II becomes thinner because of some localized disturbance (as shown in Fig. 11), the electric field $\tilde{E}$ in this region becomes intense which, in turn, creates a high Maxwell pressure spot, see Fig. 11. This high-pressure spot drives the liquid away from it, the layer nearby the spot becomes very thin and the Maxwell pressure increases again, providing positive feedback. This mechanism of instability is expected to be stabilized by viscosity at short length scales.

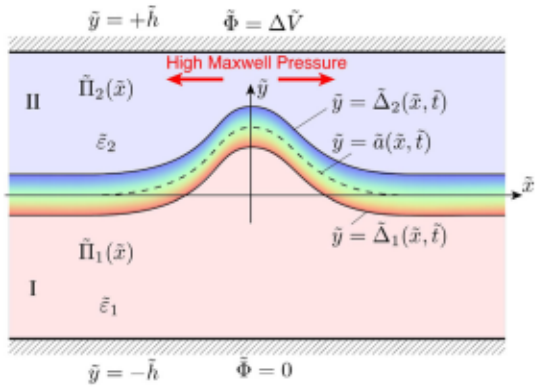

Fig. 11 Simplified sketch for the mechanism of instability of Fig. 7

The behavior described above is perfectly confirmed with DNS for initial stages of evolution at $\Lambda > \Lambda^*$, see Fig. 12a. However, whenever the assumption (56) fails (Λ is small or t is large), the resulting distribution becomes different, see Fig. 12b, c.

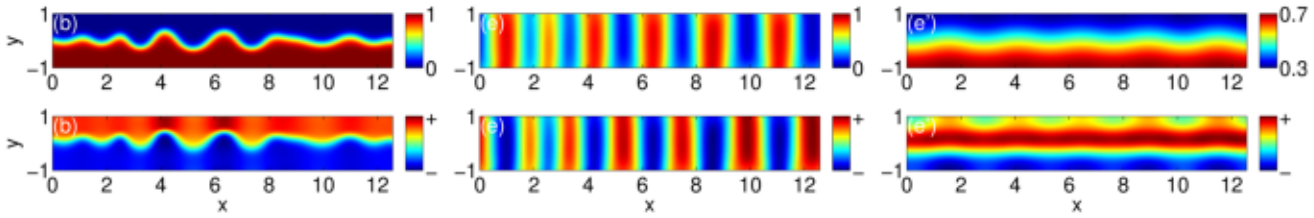

Fig. 12 Fraction (w) and Maxwell pressure distribution for $\Lambda = 32{,}000$ (**b**, **e**) and $\Lambda = 4000$ (**e**′). The snapshots are marked according to Fig. 7.

5 Conclusion

Mixing of dielectric miscible viscous liquids with different permittivities has been investigated analytically and numerically. Since the mixing layer is expanding with time, its instability is not described by the usual exponential law, but rather by the power law. This layer has been proven to be stable with respect to short- and long-wave disturbances. Intermediate waves have been found to be unstable for a finite period of time. The influence of walls does not allow to see the end of instability in practice, but the initial period, when all perturbations decay, has been confirmed with DNS. We have found by numerical simulations that with a strong enough electric field the amplitude of the waves grows, so that their edges reach the walls. Due to the Maxwell pressure between the top of the wave and the wall, the liquids reorganize into alternating stripes. This scenario of distinct stripes has not, to our knowledge, been identified previously, and our simplified theory has explained it. Mixing is enhanced with higher applied electric field as expected. However, the "stripes" of separated liquids may slow down the mixing, so moderate fields lead to better mixing in the long-time process. Moreover, we have verified that our results are consistent with experiments from [43] with transformer and silicone oils with respect to the mixing index and time evolution of instability. The obtained results can be used in microfluidic applications as, for example, the control over on-chip assays that require rapid mixing of fluids.

Acknowledgements The investigation of the self-similar solution and its linear stability analysis were supported by the Russian Science Foundation, project N 20-79-00044, and the direct numerical simulation was supported by "Projets de Recherche Conjoints" (PRCCNRS). The research is carried out using the equipment of the shared research facilities of HPC computing resources at Lomonosov Moscow State University.

References

1. S.R. Deshmukh, D.G. Vlachos, AIChE J. **51**, 3193 (2005)
2. J.S.H. Lee, D. Li, Microfluid. Nanofluid. **2**, 361 (2006)
3. Y. Gao, T.N. Wong, C. Yang, K.T. Ooi, Colloids Surfaces Physicochem. Eng. Asp. **266**, 117 (2005)
4. Y. Gao, T.N. Wong, C. Yang, K.T. Ooi, J. Colloids Interface Sci. **284**, 306 (2005)
5. C.J. Campbell, B.A. Grzybowski, Philos. Trans. R. Soc. Lond. A: Math. Phys. Eng. Sci. **362**, 1069 (2004)
6. L. Haiwang, T.N. Wong, N.-T. Nguyen, Int. J. Heat Mass Tran **53**, 772 (2010)
7. V.M. Ugaz, R.D. Elms, R.C. Lo, F.A. Shaikh, M.A. Burns, Philos. Trans. R. Soc. Lond. A: Math. Phys. Eng. Sci. **362**, 1105 (2004)
8. T.M. Squires, M.Z. Bazant, Induced-charge electro-osmosis. J. Fluid Mech. **509**, 217 (1999)
9. D.L. Zhang, S. Liu, M. Puerto, C.A. Miller, G.J. Hirasaki, J. Petrol. Sci. Eng. **52**, 213 (2006)
10. S.K. Griffiths, R.H. Nilson, Anal. Chem. **78**, 8134 (2006)
11. A. Bandopadhyaya, S. Hardt, Phys. Fluids **29**, 124101 (2017)
12. J.-L. Chen, W.-H. Shih, W.-H. Hsieh, Sens. Actuators B Chem. **188**, 11–21 (2013)
13. G. Orsi, M. Roudgar, E. Brunazzi, C. Galletti, R. Mauri, Chem. Eng. Sci. **95**, 174–183 (2013)
14. Ch.Y. Lim, YCh. Lam, Microfluid. Nanofluid. **12**, 127–141 (2012)
15. H. Sugioka, Phys. Rev. E **81**, 036306 (2010)
16. H. Lin, B.D. Storey, M.H. Oddy, C.-H. Chen, J.G. Santiago, Phys. Fluids **16**(6), 301–311 (2004)
17. C. Chen, H. Lin, S. Lele, J. Santiago, J. Fluid Mech. **524**, 263–303 (2005)
18. B.D. Storey, B.S. Tilley, H. Lin, J.G. Santiago, Phys. Fluids **17**, 018103 (2005)
19. J.D. Posner, J.G. Santiago, J. Fluid Mech. **555**, 1–42 (2006)
20. J.D. Posner, C.L. Perez, J. G. Santiago, PNAS Early Edition (2012), pp. 1–4
21. Y. Suh, S. Kang, Micromachines **1**, 82–111 (2010)
22. A. Nigam, E.B. Nauman, Trans. IChemE Part A Chem. Eng. Res. Design **83**(A7), 777–781 (2005)
23. E.B. Nauman, A. Nigam, Trans. IChemE **85**(A5), 612–615 (2007)
24. D. Bothe, C. Stemich, H.-J. Warnecke, Chem. Eng. Sci. **61**, 2950–2958 (2006)
25. F. Zoueshtiagh, S. Amiroudine, R. Narayanan, J. Fluid Mech. **628**, 43–55 (2009)
26. S. Amiroudine, F. Zoueshtiagh, R. Narayanan, Phys. Rev. E **85**, 016326 (2012)
27. S.V. Diwakar, F. Zoueshtiagh, S. Amiroudine, R. Narayanan, Phys. Fluids **27**, 084111 (2015)
28. J.F. Hoburg, J.R. Melcher, Phys. Fluids **20**, 903 (1977)
29. J.R. Melcher, G.I. Taylor, Ann. Rev. Fluids **1**, 111 (1969)

30. J.R. Melcher, *Continuum Electromechanics* (MIT Press, Cambridge, 1981)
31. D.A. Saville, Annu. Rev. Fluid Mech. **29**, 401–426 (1997)
32. J.C. Baygents, F. Baldessari, Phys. Fluids **10**, 301–311 (1998)
33. M.H. Oddy, J.G. Santiago, J.C. Mikkelsen, Anal. Chem. **73**, 5822–5832 (2001)
34. S. Di Fraia, N. Massarotti, P. Nithiarasu, Modelling electro-osmotic flow in porous media: a review. Int. J. Numer. Methods Heat Fluid Flow **28**, 472–497 (2018)
35. I. Rubinstein, B. Zaltzman, Electro-osmotically induced convection at a permselective membrane. Phys. Rev. E **62**, 2238–2251 (2000)
36. W. Liu, Y. Zhou, P. Shi, Shear electroconvective instability in electrodialysis channel under extreme depletion and its scaling laws. Phys. Rev. E **101**, 043105 (2020)
37. P. Shi, W. Liu, Length-dependent instability of shear electroconvective flow: from electroconvective instability to Rayleigh–Bénard instability. J. Appl. Phys. **124**, 204304 (2018)
38. J.F. Hoburg, J.R. Melcher, Electrohydrodynamic mixing and instability induced by co-linear fields and conductivity gradients. Phys. Fluids **20**, 903–911 (1977)
39. M. Jalaal, B. Khorshidi, E. Esmaeilzadeh, Electrohydrodynamic (EHD) mixing of two miscible dielectric liquids. Chem. Eng. J. **219**, 118–123 (2013)
40. M.-H. Chang, A.-C. Ruo, F. Chen, J. Fluid Mech. **634**, 191 (2009)
41. S. Sharan, P. Gupta, S.S. Bahga, Phys. Rev. E **95**, 023103 (2017)
42. C.C. Lin, *The Theory of Hydrodynamic Instability* (Cambridge University Press, Cambrige, 1967)
43. P.G. Drazin, W.H. Reid, *Hydrodynamic Stability*, 2nd edn. (Cambridge Mathematical Library, Cambridge, 2004)
44. Y.M. Shtemler, Dokl. Phys. **16**(4), 601–605 (1979)
45. A. Kheniene, A. Vorobev, Phys. Rev. E **88**, 022404 (2013)
46. E.A. Demekhin, S.V. Polyanskikh, Y.M. Shtemler, e-print arXiv: 1001.4502
47. E.A. Demekhin, V.S. Shelistov, S.V. Polyanskikh, Phys. Rev. E **84**, 036318 (2011)
48. M.C. Cross, P.G. Hohenberg, Rev. Mod. Phys. **65**(3), 851 (1993)
49. E.A. Demekhin, N.V. Nikitin, V.S. Shelistov, Phys. Fluids **25**, 122001 (2013)
50. N. Nikitin, Int. J. Numer. Methods Fluids **51**, 221–233 (2006)